

Jin-Ho Choi, Ki-Hyun Jeon, and Hyung-Yoon Kim

## 31.1 The Need of Non-invasive Physiological Assessment

Despite highly advanced technologies and devices in invasive physiological modalities, there is still enormous clinical need of non-invasive physiological assessment as follows. First, indirect assessment of physiological parameters is based on the profound understanding of coronary pathophysiology and exact modeling of coronary physiology. For example, computational modeling of fractional flow reserve highly depends on the exact modeling of coronary circulation. Second, non-invasive assessment enables a large-scale or population-scale study of coronary physiology which might be limited by invasive physiological assessment. Third, non-invasive physiological assessment before sending the patients to catheterization procedure might find out patients who

would not benefit from invasive angiography or physiological study and reduce unnecessary procedure. Finally, replacing invasive physiological assessment with non-invasive technology might greatly reduce the burden of medical cost.

Coronary computed tomography angiography (CCTA) is the best non-invasive modality that depicts anatomy of coronary artery. However, anatomical stenosis is a poor predictor of physiological severity and frequently underestimates or overestimates physiological severity of stenosis. Fractional flow reserve (FFR)  $< 0.80$ , a widely accepted gold standard of vessel-specific physiologically significant stenosis which may evoke myocardial ischemia, is identified in less than a half of vessel with significant stenosis defined by diameter stenosis (DS)  $\geq 50\%$ , and the discordance between anatomical stenosis and physiological severity is found as high as 40% [1, 2]. The key role of coronary artery is supplying sufficient blood flow that contains vital materials such as oxygen or glucose required by myocardium. Therefore, the insufficiency of blood supply can be defined by decreased myocardial perfusion, decreased pressure gradient or arterial flow across stenosis, or relative ratio of minimal luminal area which represents the maximal blood supply to the subtended myocardial mass. These concepts constitute the principles of non-invasive assessment of myocardial ischemia (Fig. 31.1).

---

J.-H. Choi (✉)

Departments of Emergency Medicine and Internal Medicine, Samsung Medical Center, Sungkyunkwan University School of Medicine, Seoul, South Korea  
e-mail: [jhchoimd@gmail.com](mailto:jhchoimd@gmail.com)

K.-H. Jeon

Department of Medicine, Sejong General Hospital, Bucheon, South Korea

H.-Y. Kim

Department of Medicine, Jeju National University Hospital, Jeju National University College of Medicine, Jeju, South Korea

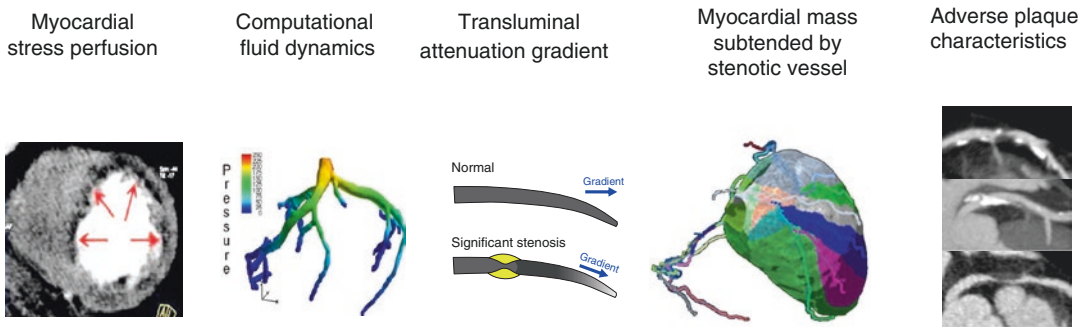


**Fig. 31.1** Concepts for non-invasive assessment of myocardial ischemia

## 31.2 Perfusion CT

The strength of perfusion imaging is visualizing the myocardial blood flow on which myocardial metabolism depends. Perfusion MR uses similar concept used in nuclear perfusion imaging or perfusion cardiac magnetic resonance imaging (CMR). From the myocardial and left ventricular cavity arterial input function or time-attenuation curves, the extent of regional myocardial perfusion is calculated or compared with the other regional myocardial perfusion. Perfusion is imaged in a complete cardiac cycle (dynamic perfusion imaging) or as a snapshot (static perfusion imaging). Scanners equipped with dual energy source can be used for perfusion imaging and mostly used for static perfusion imaging (Fig. 31.2). The performance of perfusion CT for predicting functionally significant stenosis is considered to be similar to nuclear perfusion imaging, stress CMR, or stress echocardiography, and is being validated against FFR [3–5]. Standard coronary angiography can be done along with perfusion imaging, which enables simultaneous anatomic evaluation of coronary arteries with functional evaluation of heart. Therefore, perfusion CT combined with coronary CT angiography can be a one-stop shop modality that assesses both anatomical and functional stenosis within a single session [6].

### 31.2.1 Technical Aspect of Perfusion CT Imaging

Hyperemia is induced by pharmacological stress agents. Intravenous adenosine is widely used in a continuous dose of 140  $\mu\text{g}/\text{kg}/\text{min}$  for 2 or 3 min. Regadenoson has longer plasma half time than adenosine and is administered in a single agent. Also it is a selective adenosine 2A receptor agonist and can be used in patients with asthma or airway disease. Dobutamine, a myocardial beta-1 agonist, or dipyridamole, adenosine receptor blocker, is not commonly used (Table 31.1).

Static or snap-shot perfusion CT assesses myocardial contrast distribution in a single time and doable in most CT scanners with lesser radiation exposure to dynamic perfusion CT. With sophisticated mathematical modeling, dynamic perfusion CT enables direct quantification of myocardial blood flow (MBF), myocardial blood volume, and myocardial flow reserve (Table 31.2). Regarding the diagnostic performance, static perfusion CT showed sensitivity = 0.85 (95% confidence interval = 0.70–0.93), specificity = 0.81 (0.59–0.93), area under curve = 0.90 (0.87–0.92) [7]. A recent dynamic perfusion CT showed comparable performance compared to CMR (Table 31.3) [8–20]. Also perfusion CT is better suited for quantification of myocardial blood flow than perfusion MR. Based on the nuclear perfusion studies, the nominal value of resting myocardial blood flow is

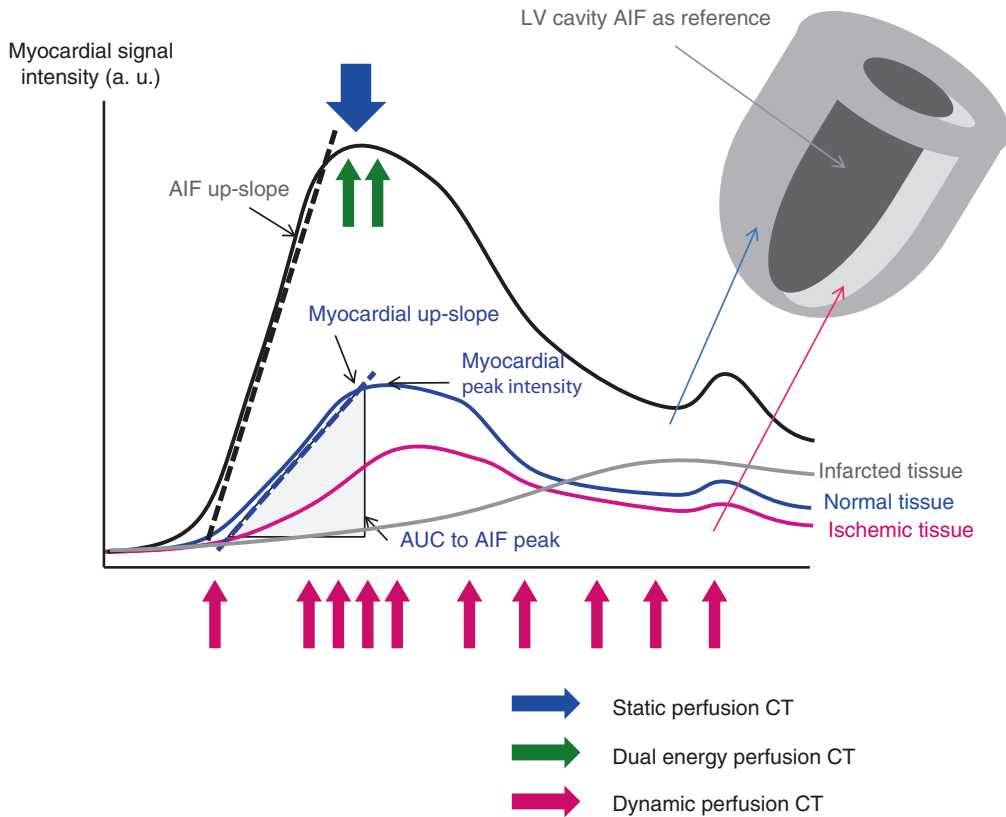


**Fig. 31.2** Principle of myocardial perfusion CT. The difference between myocardial blood flow correlates with the myocardial up-slope normalized by arterial input function (AIF) up-slope, area under curve (AUC) of myocardial signal intensity up to AIF peak, or myocardial peak signal intensity. The difference between normal tissue and ischemic tissue is imaged as perfusion defect (line with red arrows)

**Table 31.1** Stress agents for perfusion imaging

	Advantage	Disadvantage
Exercise	Most physiological	Motion artifact → not practical for CT or MR
	Least expensive	Effort-dependent
Adenosine	Current de facto standard	Potential bronchospasm (not good for chronic obstructive lung disease, asthma, caffeine user) Tachycardia, AV block
Dipyridamole	Inexpensive	Prolonged effect Tachycardia, AV block May require aminophylline
Regadenoson, binodenoson	Bolus injection	Expensive
	Fewer side effects in COPD/asthma	Prolonged effect Tachycardia
Dobutamine	Physiological	Lower sensitivity/specificity Tachycardia Can provoke ischemia

**Table 31.2** Techniques for myocardial perfusion CT

	Strength	Weak points
Static perfusion CT	• Doable in most CT scanner	• Highly affected by image acquisition timing
	• Doable with standard CCTA	
	• Minimal radiation (1–3 mSv)	• May need multiphase reconstruction to reduce artifacts (beam hardening, motion, partial scan artifacts)
	• TPR (trans-myocardial perfusion ratio)	
Dynamic perfusion CT	• Less susceptible to artifact	• Need specific scanner (256 or 320-slice, or 128-slice with shuttle mode)
	• Quantitative blood flow analysis (myocardial blood flow or flow reserve)	• High radiation (>10 mSv)
		• Axial coverage might be insufficient
		• Need separated CCTA scanning
		• Limited clinical data
Dual energy perfusion CT	• Iodine distribution map → better tissue discrimination	• Affected by image acquisition timing
	• Quantitation of myocardial blood pool	• Needs standardization of iodine map interpretation
		• Mostly static perfusion CT

known to be 0.9 ml/μg/min. The cut-off value of hemodynamically significant stenosis in perfusion CT was reportedly 0.75–0.78 ml/μg/min [16].

### 31.3 Computational Simulation of Fractional Flow Reserve

Increase of myocardial blood flow by 2 to 3-fold is required to match the increased need of cardiac output in most activities. Coronary microvessel accounts for most resistance or pressure drop in coronary circulation. The increase of myocardial blood flow is mainly controlled by decrease in microvascular resistance. Therefore functionally significant epicardial coronary artery stenosis can be defined by failure to increase blood flow during hyperemia which induces maximal dilatation of resistance vessel. Fractional flow reserve (FFR) is defined by the ratio of hyperemic coronary flow through stenotic vessel to the hypothetical normal vessel. Because flow is proportional to pressure in fixed stenosis, FFR can be measured by average pressure gradient. Pressure drop of more than 20% or  $FFR \leq 0.80$  is widely advocated as a gold standard of vessel-specific physiologically significant stenosis which may evoke myocardial ischemia.

FFR is measured during invasive cardiac catheterization and requires insertion of a pressure wire inserted through the stenosis. There may be and instability of measurement and signal shift. Placement of a pressure wire near the stenosis or pressure recovery zone may lead to overestimation of FFR. A non-invasive simulation of FFR would be very valuable to avoid these procedural shortcomings and the expense of pressure wire and invasive cardiac catheterization.

#### 31.3.1 Computation of Simulated FFR

Like the other fluid systems, blood flow in the cardiovascular system is ruled by the physical laws of mass conservation, momentum conservation, and energy conservation. Therefore it can be calculated by mathematical models. For patient-specific coronary circulation, 3-dimensional numerical models based on computational flow dynamics which can compute complex flow patterns are preferred to zero dimensional models or lumped parameter model which is employed in large systemic vessels. Computational FFR is derived based on the regional physical geometry, the boundary condition which is the behavior and

**Table 31.3** Diagnostic performance of perfusion CT

Study and publication	Techniques (Scanner)	N	Reference	Stenosis (%)	Sensitivity	Specificity	PPV	NPV	Basis of analysis
Rocha-Filho et al. [8]	Static (64-DSCT)	35	ICA	50	91	91	86	93	Vessel
				70	91	78	53	97	
Feuchtnr et al. [9]	Static (128-DSCT)	25	ICA	70	100	74	97	100	Vessel
Nasis et al. [10]	Static (320-MDCT)	20	SPECT/ICA	50	94	98	94	98	Vessel/territory
				70	79	91	73	93	
Carrascosa et al. [11]	Static, rapid kV switching	25	SPECT	–	73	95	–	–	Vessel
Magalhaes et al. [12]	Static (320-MDCT)	381	ICA + SPECT,MR	50	98	96	98	96	Territory
					58	86	87	55	Vessel
Huber et al. [13]	Static (256-MDCT)	32	ICA	50	76	100	90	100	Vessel
Rossi et al. [14]	Dynamic (128-DSCT)	80	ICA	50	78	75	91	51	Territory
					88	90	98	77	Vessel
Bamberg et al. [15]	Dynamic (128-DSCT)	33	FFR	50	93	87	75	97	Vessel
Bamberg et al. [16]	Dynamic (128-DSCT)	31	Cardiac MR	–	100	75	100	92	Vessel
Ko et al. [17]	Dynamic (64-DSCT)	45	ICA	50	93	86	88	91	Vessel
Wang et al. [18]	Dynamic (128-DSCT)	30	ICA/SPECT	50	90	81	58	97	Vessel/territory
Kim et al. [19]	Dynamic (128-DSCT)	50	Cardiac MR	–	77	94	53	98	Vessel/territory
Wichmann et al. [20]	Dynamic (128-DSCT)	71	Visual assessment	50	100	88	100	43	Territory

properties at the boundaries of the region, and the physical laws of fluid in the region.

FFR can be described as a pressure gradient across stenotic segment during maximal hyperemia. Anatomical stenosis, myocardial mass, and microvascular resistance constitute FFR value and can be calculated from patient-specific sophisticated coronary arterial anatomical model, vessel-specific myocardial mass, and microvascular resistance which determine the outlet boundary condition [21, 22]. CT images provide patient-specific anatomy model of local geometry, individual coronary artery morphology, volume, and myocardial mass. From these data, cardiac output and baseline coronary blood flow can be calculated by using allometric scaling laws [23–25]. This computational approach was derived from a general model that describes the transport of essential materials through space-filling fractal branched networks, and is based on a form-function relationship [26]. The diameter-flow rate relation is determined according to Murray’s law [27] and Poiseuille’s equation, which considers shear stress on the endothelial surface and remodeling to maintain homeostasis [28]. Morphometry laws are also adapted to obtain the physiological resistance to flow aroused by coronary artery branches [29].

Microvascular resistance at baseline and during maximal hyperemia, which is fundamental for FFR measurement, can be approximated using population-based data on the effect of adenosine on coronary flow [30] (Fig. 31.3).

### 31.3.2 Clinical Results of Computational FFR

Landmark trials including DISCOVER-FLOW [31], DeFACTO [32], and NXT [33] showed that FFR-CT, a proprietary computational FFR, showed high diagnostic performance in discriminating ischemia in patients who had intermediate coronary artery stenosis. The NXT trial reported sensitivity and negative predictive value of FFR-CT in diagnosis of ischemia (defined as invasive FFR < 0.80) in patients with intermediate stenosis severity were 80% and 92%, respectively [33]. In a recent meta-analysis of FFR-CT based on 833 patients and 1377 vessels, FFR-CT showed a moderate diagnostic performance for identification of ischemic vessel with pooled sensitivity = 84% and specificity = 76% at a per-vessel basis [34] (Table 31.4). The PLATFORM study showed that a decision-making strategy

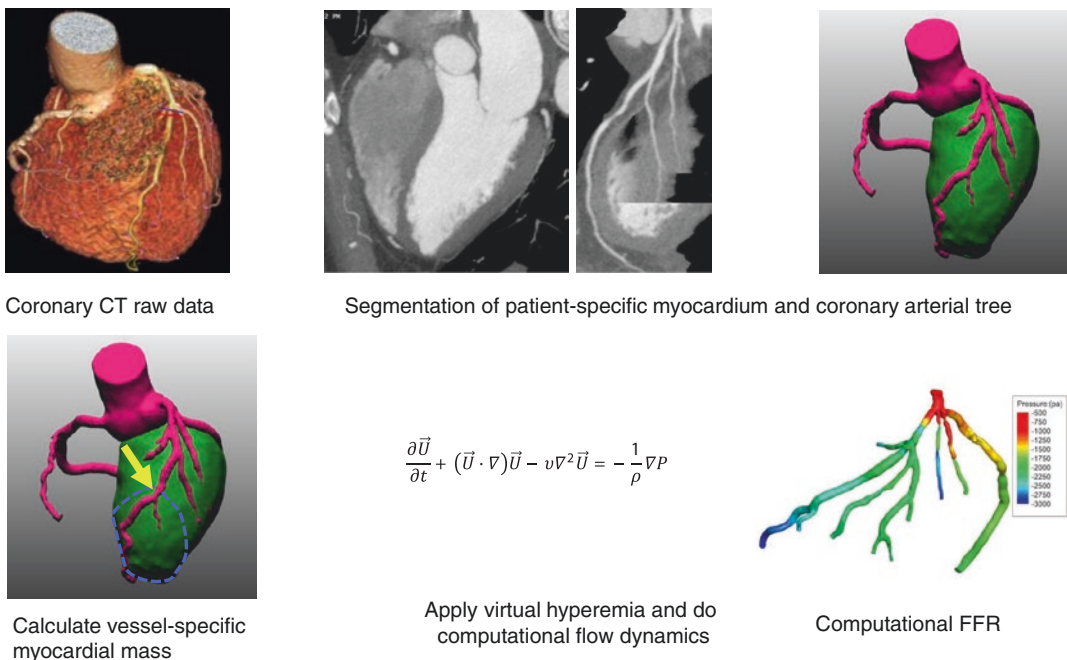


**Fig. 31.3** Concept of computational FFR

**Table 31.4** Results of non-invasive computational FFR technologies

Study	Technology	N of vessels	Sensitivity (%)	Specificity (%)	PPV (%)	NPV (%)	Accuracy (%)	Area under curve, per vessel	Correlation coefficient compared with FFR	Computation time
FFR-CT, DISCOVER-FLOW, Koo et al. [31]	Heartflow ver 1.0	159	88	82	74	92	84	0.90	0.72	Hours, off-site
FFR-CT, DeFACTO, Min et al. [32]	Heartflow ver 1.2	408	80	63	56	84	69	0.81	0.63	Hours, off-site
FFR-CT, NXT, Norgaard et al. [33]	Heartflow ver 1.4	484	84	87	62	95	86	0.93	0.82	Hours, off-site
FFR-CT, Kim et al. [19]	Heartflow ver 1.2	48	85	57	83	62	77	–	0.60	Hours, off-site
cFFR	Siemens cFFR ver 1.4	67	85	85	71	93	85	0.92	0.66	<1 h, standalone
cFFR	Siemens cFFR ver 1.4	189	88	65	65	88	75	0.83	0.59	<1 h, standalone
cFFR	Siemens cFFR ver 1.7	23	83	76	56	93	78	–	0.77	<1 h, standalone
Pooled analysis	–	1330	84	76	63	91	79	0.86	–	–

Per-vessel data is shown. PPV positive predictive value, NPV negative predictive value

using CCTA with FFR-CT was associated with clinical outcomes comparable to using invasive FFR and a 33% cost reduction [35]. Therefore, FFR-CT can effectively rule out intermediate lesions that cause ischemia and could also reduce the unnecessary ICA and invasive FFR.

### 31.4 Intracoronary Transluminal Attenuation Gradient Analysis

#### 31.4.1 Transluminal Attenuation Gradient (TAG) and Corrected Contrast Opacification (CCO)

Standard coronary CT image is a snapshot of dynamic transit of intravascular contrast driven by blood flow. Therefore, coronary CT is not only a simple static anatomical imaging but also contains information of coronary hemodynamics. Intracoronary contrast filling is governed by arterial input function from coronary ostium and the flow or velocity of intracoronary flow. Based on this intuitive concept, transluminal attenua-

tion gradient (TAG) was defined as the difference of intracoronary attenuation along vessel axis that reflects contrast kinetics and is readily available from conventional CCTA image without additional radiation or off-site long time computation [36]. TAG theoretically depends on the temporal uniformity of Z-axis coverage and adequate contrast enhancement curve (Fig. 31.4). TAG has been tested in both animal and human studies and showed consistently poor correlation with anatomical and functional stenosis [37–42]. Adjustment with descending aortic opacification (corrected contrast opacification, CCO) or exclusion of nonlinear values caused by stented or calcified segment has been proposed but with mixed results [38, 42, 43]. Because coronary CT image is a snapshot of convection of intracoronary time-varying contrast bolus, TAG represents the spatial dispersion of contrast concentration along vessel axis. Therefore, the discordance among TAG and anatomical or functional stenosis is no wonder considering the well-known discordance among anatomical stenosis, fractional flow reserve (FFR), and coronary flow reserve (CFR).

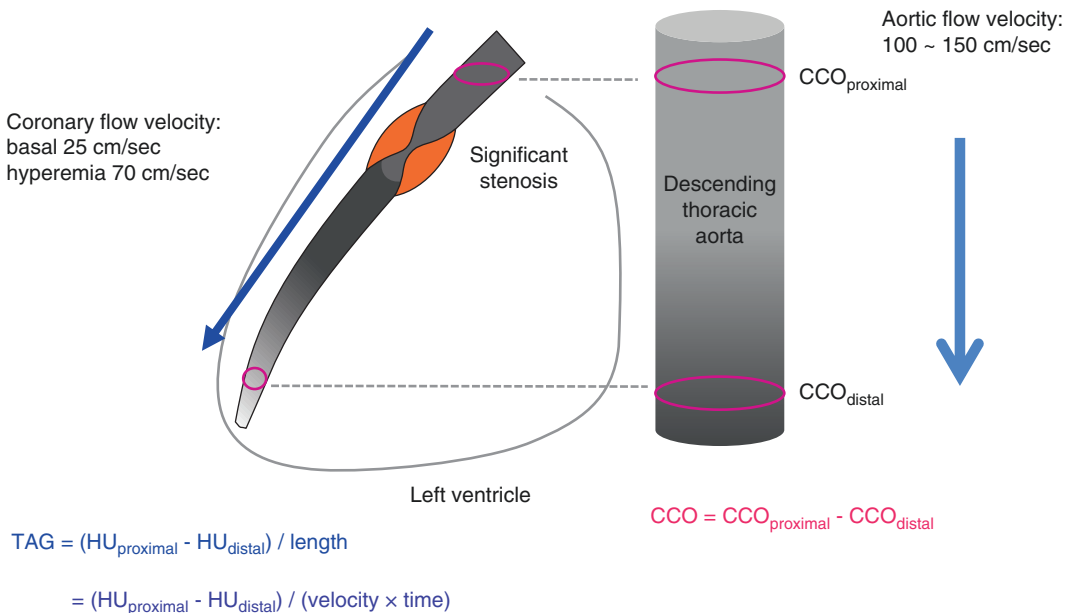


**Fig. 31.4** Concept of transluminal attenuation gradient (TAG) and corrected contrast opacification (CCO)



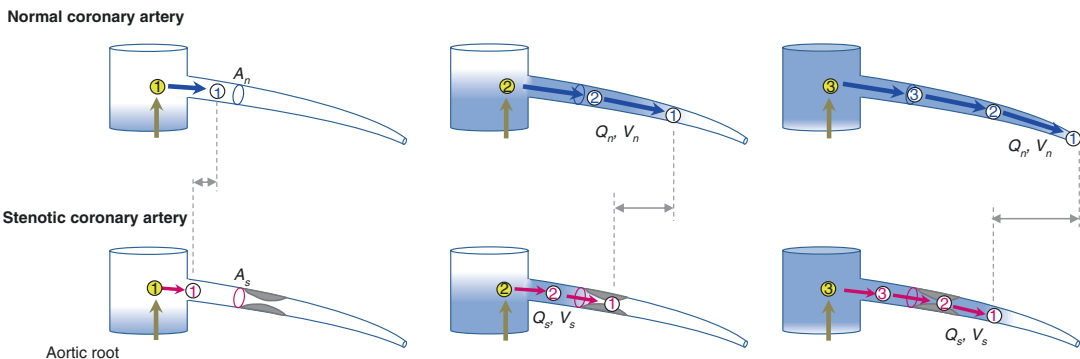
### 31.4.2 Transluminal Attenuation Flow Encoding (TAFE)

The principle of myocardial blood flow assessment in perfusion scan based on the comparison of enhancement dynamics between left ventricular cavity and myocardium can be applied with modification to standard CCTA data [44, 45]. This concept enables calculation of CBF from the time-dependent change of contrast density proximal to coronary artery as input function of contrast cohort, arterial volume to be filled by the contrast cohort, and the gradient of intraluminal contrast density which reflects blood flow velocity. All these input parameters are readily and rapidly available from current conventional CT suite [46]. Based on this concept, Lardo et al. reported an elegant engineering solution named transluminal attenuation flow encoding (TAFE) (Fig. 31.5) [47]. Coronary CT image is a snapshot of convection of intracoronary time-varying contrast bolus. Therefore TAG represents the spatial dispersion of contrast concentration along vessel axis. With additional temporal data from arterial input function, TAFE formula decodes the spatial dispersion of TAG into temporal dispersion of vessel-specific CBF. TAFE showed excellent correlation with myocardial blood flow (MBF) in animal microsphere model and warrants validation in human study.

### 31.5 Coronary Artery Stenosis and Subtended Myocardial Mass

FFR is a mean pressure gradient across stenosis with maximal myocardial blood flow. Anatomical stenosis, myocardial mass, and microvascular resistance are major constituents of FFR value [21]. The major unknowns in anatomical measurement are myocardial mass and microvascular resistance. Therefore the anatomic-physiological discordance can be reduced by addition of downstream myocardial mass to anatomical stenosis of supplying artery (Fig. 31.6). Based on the fluid continuity principle, functional severity of stenosis was shown to increase proportionally to the ratio of flow demand represented by subtended myocardial mass to flow supply represented by luminal area or diameter of supplying vessel [48, 49]. Principle of efficiency or minimum energy loss concept is considered in the structure of human vascular tree and myocardial territory based on the fact that energy-efficient provision of materials such as oxygen in hierarchical fractal-like network of branching tubes plays a key role in the mechanism of living organism [50].

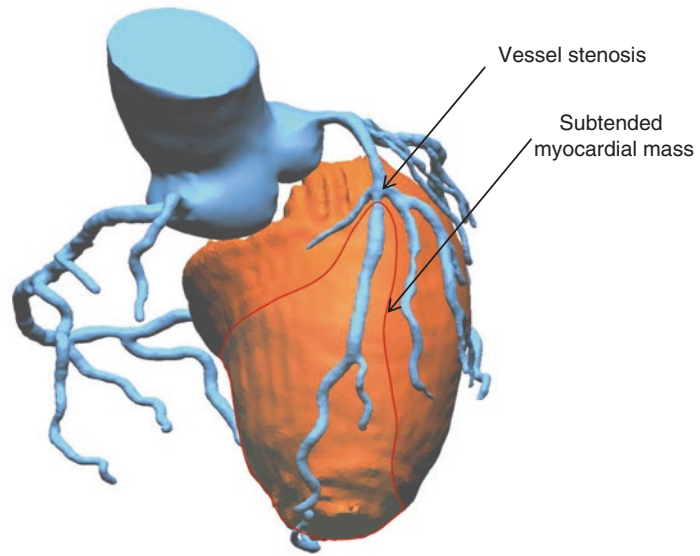
Two mathematical principles that have been used extensively in life science can be applied to calculate the relationship between vessel dimension and subtended myocardial mass (Table 31.5).



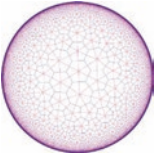

**Fig. 31.5** Concept of transluminal arterial flow encoding (TAFE). Addition of the arterial input function (AIF, yellow arrow) adds time domain to TAG ( $=\Delta HU/\text{arterial length}$ ) and enables calculation of vessel-specific coronary

blood flow. Compared to normal artery, the flow of stenotic artery is slower and has lower flow rate. Numbers in circle represent time points

**Fig. 31.6** Concept of myocardial mass subtended by the vessel



**Table 31.5** Mathematical principles for the relationship between vessel dimension and subtended myocardial mass

Methods	Principle	Mathematics
Voronoi tessellation 	Geometry and mathematics	$R_k = \{x \in X / d(x, P_k) \leq d(x, P_j) \text{ for all } j \neq k\}$
Allometric scaling law 	Hypothesis of logarithmic correlations in life science	$Y = K X_b^a$ or $\log(Y) = a \log(X) + \log K$

Voronoi tessellation is based on the geometrical characteristics of vessel course and myocardial geometry. Allometric scaling law is a simple and universally observed logarithmic relationship among size, function, and energy expenditure in life science [26]. Stem-and-crown models describing scaling power between structures and functions were developed theoretically and validated experimentally in both animal and human studies [51, 52]. In clinical study, both Voronoi- and allometric scaling law-based study showed similar findings for the relation between vessel size and subtended myocardial mass (Table 31.6) [53, 54].

The concept of myocardial mass subtended by specific coronary artery can be extended beyond vessel-specific ischemia and may lead to better diagnostic and therapeutic decision in cardiovascular medicine including the following clinical issues. It might be used for adjudicating myocardial infarction caused by supply and demand mismatch (type 2) [55]. It also may clarify the appropriateness and optimal threshold of revascularization. Direct assessment of the amount of ischemic myocardium as well as myocardium to be revascularized has been estimated semi-quantitatively by angiographic scoring systems. As the FFR could

**Table 31.6** Results of vessel dimension to subtended myocardial mass for detection of functionally significant stenosis

Study	Technology	N of vessels	Index parameter	Reference	Sensitivity (%)	Specificity (%)	PPV (%)	NPV (%)	Accuracy (%)	Area under curve, per vessel	Correlation coefficient compared with FFR
Kim et al. [53]	Allometric scaling law	724	Myocardial mass, angiographic minimal luminal diameter	FFR $\leq$ 0.80	78	72	75	75	75	0.84	0.61
Kang et al. [54]	Voronoi tessellation	103	Myocardial mass, IVUS minimal luminal area	FFR $\leq$ 0.80	88	90	86	92	90	0.94	0.78

Per-vessel data is shown. *PPV* positive predictive value, *NPV* negative predictive value

reclassify the need of revascularization based on the presence of ischemia, myocardial mass subtended by specific vessel might reclassify the strategy of revascularization based on the amount of ischemic myocardium to be saved [56–59]. The concept of vessel-specific myocardial mass explains the limited clinical benefit of bifurcation side branch and chronic total occlusion (CTO) revascularization [60], because both side branch of bifurcation and CTO vessel supply smaller or infarcted myocardial mass [61–64].

### 31.6 Limitations

The most important limitation of non-invasive physiological assessment is radiation exposure required by CT image, especially in perfusion CT imaging. A combined rest and stress myocardial perfusion CT may reach radiation dose of >15 mSv. Although the radiation exposure of CT is regarded as lower than those with nuclear imaging, appropriate radiation reducing strategy should be applied as reasonable as possible (Fig. 31.7).

Insufficient spatial and temporal resolution is the major cause of inadequate results. Typical isotropic

spatial resolution of CT image is 0.5 mm at best. Therefore even single voxel difference in 3.0 mm sized vessel results in 17% difference in diameter. Such vessel with 50% diameter stenosis would have just 7–9 voxels in the lumen. Addition or deletion of single voxel causes 33% difference in minimal luminal diameter or 11% difference in minimal luminal area (Fig. 31.8). Mathematical correction by subvoxel resolution technique and avoidance of partial volume effect is being developed.

Mismatch of perfusion defect and stenotic or non-stenotic coronary artery may occur as cardiac positron emission tomography (PET) and coronary CT. Concept of vessel-specific myocardial territory rather than traditional 17-segment model may reduce misregistration error [53, 54, 65].

Boundary conditions in computational flow dynamics are critical in the result of computational FFR but include several assumed parameters which cannot be determined from conventional coronary CT. The individual variation of blood pressure, heart rate, coronary flow reserve, extent of collateral flow may explain the discrepancy between computational FFR and invasively acquired FFR (correlation coefficient  $r = 0.72$  in DISCOVER-FLOW study) [31]. The time to calculation and

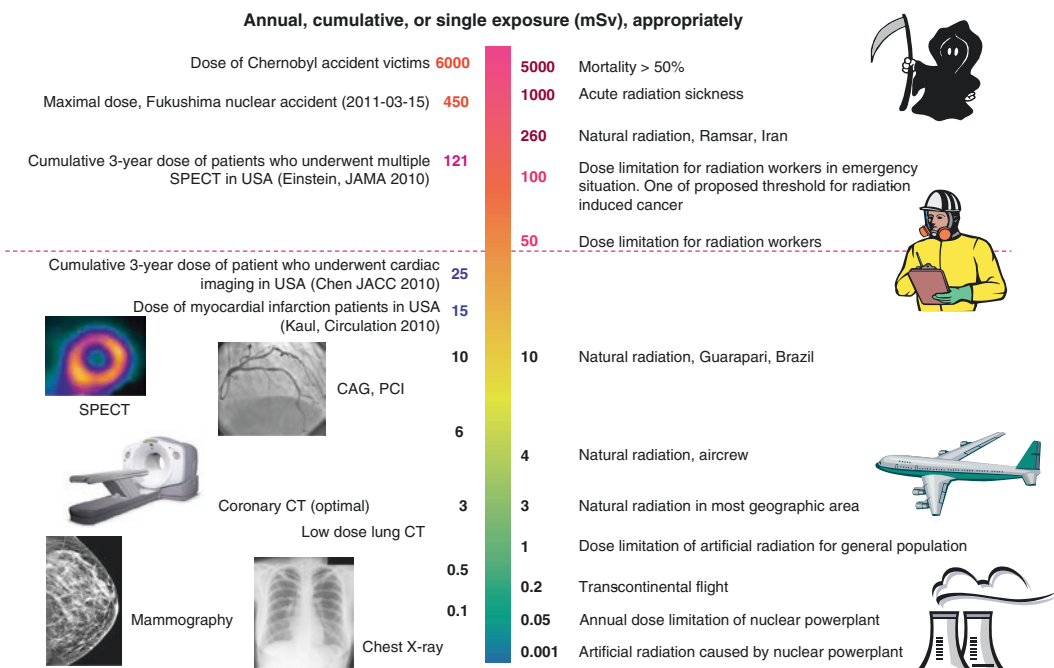
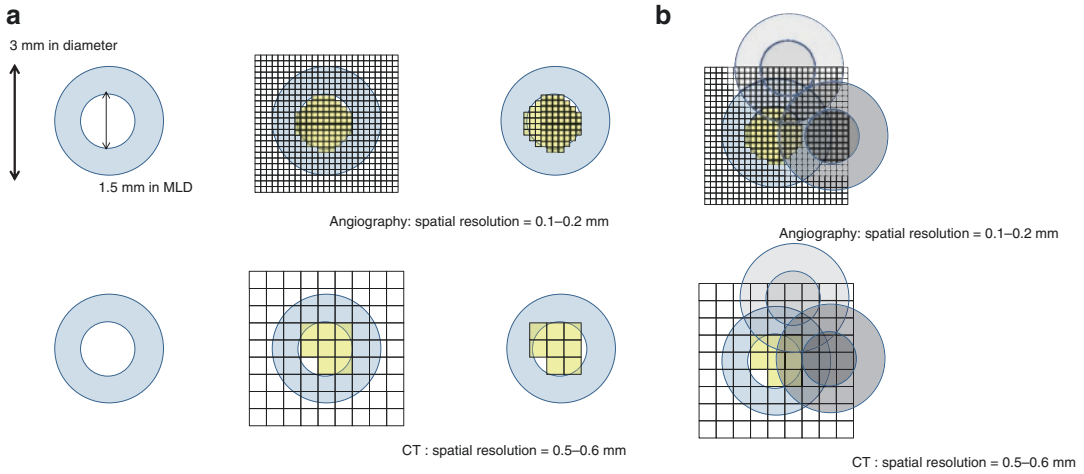
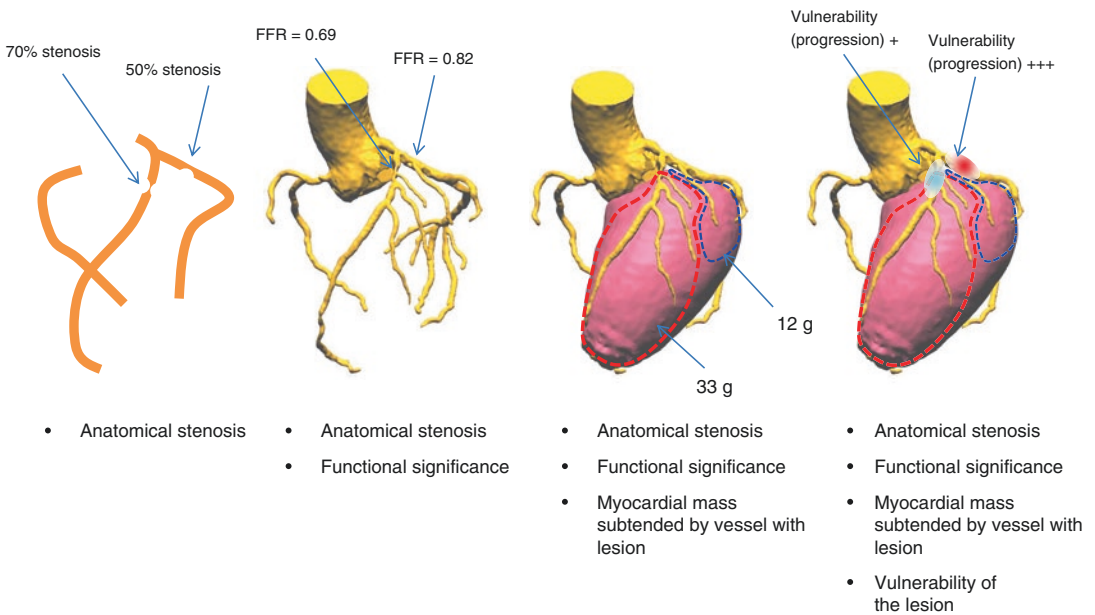


Fig. 31.7 Radiation exposure



**Fig. 31.8** Limitations in spatial resolution and motion artifact. **(a)** Less than 10 voxels consists lumen of typical coronary artery disease with 3.0 mm diameter and 50% stenosis. Omission or addition of single voxel affects significantly the result of computational FFR. **(b)** The limitation of spatial resolution may be worsen by the motion artifact



**Fig. 31.9** Multifactorial non-invasive evaluation of coronary artery disease

heavy computational resource is another limitation of computational FFR but may be overcome by big-data based machine learning [66].

Single measurement or modality may represent but cannot show every aspect of coronary artery disease and is not sufficient for decision of treatment strategy. Revascularization by percuta-

neous coronary intervention or bypass surgery relieves symptom but does not improve clinical outcome of all patients [67]. Non-invasive physiological assessment may vastly improve the predictive value of coronary artery disease evaluation and be additive to the current decision-making strategy (Fig. 31.9).

## References

- Blankstein R, Di Carli MF. Integration of coronary anatomy and myocardial perfusion imaging. *Nat Rev Cardiol.* 2010;7:226–36
- Toth G, Hamilos M, Pyxaras S, et al. Evolving concepts of angiogram: fractional flow reserve discordances in 4000 coronary stenoses. *Eur Heart J.* 2014;35:2831–8
- Yang DH, Kim YH, Roh JH, et al. Stress myocardial perfusion CT in patients suspected of having coronary artery disease: visual and quantitative analysis-validation by using fractional flow reserve. *Radiology.* 2015;276:715
- Greenwood JP, Maredia N, Younger JF, et al. Cardiovascular magnetic resonance and single-photon emission computed tomography for diagnosis of coronary heart disease (CE-MARC): a prospective trial. *Lancet.* 2012;379:453–60
- Takx RA, Blomberg BA, El Aidi H, et al. Diagnostic accuracy of stress myocardial perfusion imaging compared to invasive coronary angiography with fractional flow reserve meta-analysis. *Circ Cardiovasc Imaging.* 2015;8:e002666
- Williams MC, Newby DE. CT myocardial perfusion imaging: current status and future directions. *Clin Radiol.* 2016;71:739–49
- Sorgaard MH, Kofoed KF, Linde JJ, et al. Diagnostic accuracy of static CT perfusion for the detection of myocardial ischemia. A systematic review and meta-analysis. *J Cardiovasc Comput Tomogr.* 2016;10:450
- Rocha-Filho JA, Blankstein R, Shurman LD, et al. Incremental value of adenosine-induced stress myocardial perfusion imaging with dual-source CT at cardiac CT angiography. *Radiology.* 2010;254:410–9
- Feuchtner G, Goetti R, Plass A, et al. Adenosine stress high-pitch 128-slice dual-source myocardial computed tomography perfusion for imaging of reversible myocardial ischemia: comparison with magnetic resonance imaging. *Circ Cardiovasc Imaging.* 2011;4:540–9
- Nasis A, Ko BS, Leung MC, et al. Diagnostic accuracy of combined coronary angiography and adenosine stress myocardial perfusion imaging using 320-detector computed tomography: pilot study. *Eur Radiol.* 2013;23:1812–21
- Carrascosa PM, Deviggiano A, Capunay C, et al. Incremental value of myocardial perfusion over coronary angiography by spectral computed tomography in patients with intermediate to high likelihood of coronary artery disease. *Eur J Radiol.* 2015;84:637–42
- Magalhaes TA, Kishi S, George RT, et al. Combined coronary angiography and myocardial perfusion by computed tomography in the identification of flow-limiting stenosis - the CORE320 study: an integrated analysis of CT coronary angiography and myocardial perfusion. *J Cardiovasc Comput Tomogr.* 2015;9:438–45
- Huber AM, Leber V, Gramer BM, et al. Myocardium: dynamic versus single-shot CT perfusion imaging. *Radiology.* 2013;269:378–86
- Rossi A, Uitterdijk A, Dijkshoorn M, et al. Quantification of myocardial blood flow by adenosine-stress CT perfusion imaging in pigs during various degrees of stenosis correlates well with coronary artery blood flow and fractional flow reserve. *Eur Heart J Cardiovasc Imaging.* 2013;14:331–8
- Bamberg F, Becker A, Schwarz F, et al. Detection of hemodynamically significant coronary artery stenosis: incremental diagnostic value of dynamic CT-based myocardial perfusion imaging. *Radiology.* 2011;260:689–98
- Bamberg F, Marcus RP, Becker A, et al. Dynamic myocardial CT perfusion imaging for evaluation of myocardial ischemia as determined by MR imaging. *JACC Cardiovasc Imaging.* 2014;7:267–77
- Ko BS, Cameron JD, Leung M, et al. Combined CT coronary angiography and stress myocardial perfusion imaging for hemodynamically significant stenoses in patients with suspected coronary artery disease: a comparison with fractional flow reserve. *JACC Cardiovasc Imaging.* 2012;5:1097–111
- Wang Y, Qin L, Shi X, et al. Adenosine-stress dynamic myocardial perfusion imaging with second-generation dual-source CT: comparison with conventional catheter coronary angiography and SPECT nuclear myocardial perfusion imaging. *AJR Am J Roentgenol.* 2012;198:521–9
- Kim SM, Chang SA, Shin W, Choe YH. Dual-energy CT perfusion during pharmacologic stress for the assessment of myocardial perfusion defects using a second-generation dual-source CT: a comparison with cardiac magnetic resonance imaging. *J Comput Assist Tomogr.* 2014;38:44–52
- Wichmann JL, Meinel FG, Schoepf UJ, et al. Semiautomated global quantification of left ventricular myocardial perfusion at stress dynamic CT: diagnostic accuracy for detection of territorial myocardial perfusion deficits compared to visual assessment. *Acad Radiol.* 2016;23:429–37
- Gould KL, Johnson NP, Bateman TM, et al. Anatomic versus physiologic assessment of coronary artery disease. Role of coronary flow reserve, fractional flow reserve, and positron emission tomography imaging in revascularization decision-making. *J Am Coll Cardiol.* 2013;62:1639–53
- Min JK, Taylor CA, Achenbach S, et al. Noninvasive fractional flow reserve derived from coronary CT angiography: clinical data and scientific principles. *JACC Cardiovasc Imaging.* 2015;8:1209–22
- Choy JS, Kassab GS. Scaling of myocardial mass to flow and morphometry of coronary arteries. *J Appl Physiol.* 2008;104:1281–6
- Kassab GS. Scaling laws of vascular trees: of form and function. *Am J Physiol Heart Circ Phys.* 2006;290:H894–903
- Lindstedt SL, Schaeffer PJ. Use of allometry in predicting anatomical and physiological parameters of mammals. *Lab Anim.* 2002;36:1–19
- West GB, Brown JH, Enquist BJ. A general model for the origin of allometric scaling laws in biology. *Science.* 1997;276:122–6

27. Murray CD. The physiological principle of minimum work: I. The vascular system and the cost of blood volume. *Proc Natl Acad Sci U S A*. 1926; 12:207–14
28. Kamiya A, Togawa T. Adaptive regulation of wall shear stress to flow change in the canine carotid artery. *Am J Phys*. 1980;239:H14–21
29. Wischgoll T, Choy JS, Kassab GS. Extraction of morphology and branching angles of porcine coronary arterial tree from CT images. *Am J Physiol Heart Circ Physiol*. 2009;297:H1949–55
30. Wilson RF, Wyche K, Christensen BV, Zimmer S, Laxson DD. Effects of adenosine on human coronary arterial circulation. *Circulation*. 1990;82:1595–606
31. Koo BK, Erglis A, Doh JH, et al. Diagnosis of ischemia-causing coronary stenoses by noninvasive fractional flow reserve computed from coronary computed tomographic angiograms. Results from the prospective multicenter DISCOVER-FLOW (diagnosis of ischemia-causing Stenoses obtained via noninvasive fractional flow reserve) study. *J Am Coll Cardiol*. 2011;58:1989–97
32. Min JK, Leipsic J, Pencina MJ, et al. Diagnostic accuracy of fractional flow reserve from anatomic CT angiography. *JAMA*. 2012;308:1237–45
33. Norgaard BL, Leipsic J, Gaur S, et al. Diagnostic performance of noninvasive fractional flow reserve derived from coronary computed tomography angiography in suspected coronary artery disease: the NXT trial (analysis of coronary blood flow using CT angiography: next steps). *J Am Coll Cardiol*. 2014;63:1145–55
34. Wu W, Pan DR, Foin N, et al. Noninvasive fractional flow reserve derived from coronary computed tomography angiography for identification of ischemic lesions: a systematic review and meta-analysis. *Sci Rep*. 2016;6:29409
35. Douglas PS, De Bruyne B, Pontone G, et al. 1-year outcomes of FFRCT-guided care in patients with suspected coronary disease: the PLATFORM study. *J Am Coll Cardiol*. 2016;68:435–45
36. Choi JH, Min JK, Labounty TM, et al. Intracoronary transluminal attenuation gradient in coronary CT angiography for determining coronary artery stenosis. *JACC Cardiovasc Imaging*. 2011;4:1149–57
37. Choi JH, Kim EK, Kim SM, et al. Noninvasive evaluation of coronary collateral arterial flow by coronary computed tomographic angiography. *Circ Cardiovasc Imaging*. 2014;7:482–90
38. Stuijzand WJ, Danad I, Raijmakers PG, et al. Additional value of transluminal attenuation gradient in CT angiography to predict hemodynamic significance of coronary artery stenosis. *JACC Cardiovasc Imaging*. 2014;7:374–86
39. Wong DT, Ko BS, Cameron JD, et al. Comparison of diagnostic accuracy of combined assessment using adenosine stress computed tomography perfusion + computed tomography angiography with transluminal attenuation gradient + computed tomography angiography against invasive fractional flow reserve. *J Am Coll Cardiol*. 2014;63:1904–12
40. Steigner ML, Mitsouras D, Whitmore AG, et al. Iodinated contrast opacification gradients in normal coronary arteries imaged with prospectively ECG-gated single heart beat 320-detector row computed tomography. *Circ Cardiovasc Imaging*. 2010;3:179–86
41. Yoon YE, Choi JH, Kim JH, et al. Noninvasive diagnosis of ischemia-causing coronary stenosis using CT angiography: diagnostic value of transluminal attenuation gradient and fractional flow reserve computed from coronary CT angiography compared to invasively measured fractional flow reserve. *JACC Cardiovasc Imaging*. 2012;5:1088–96
42. Choi JH, Koo BK, Yoon YE, et al. Diagnostic performance of intracoronary gradient-based methods by coronary computed tomography angiography for the evaluation of physiologically significant coronary artery stenoses: a validation study with fractional flow reserve. *Eur Heart J Cardiovasc Imaging*. 2012;13:1001–7
43. Chow BJ, Kass M, Gagne O, et al. Can differences in corrected coronary opacification measured with computed tomography predict resting coronary artery flow? *J Am Coll Cardiol*. 2011;57:1280–8
44. Gewirtz H, Dilsizian V. Integration of quantitative positron emission tomography absolute myocardial blood flow measurements in the clinical management of coronary artery disease. *Circulation*. 2016;133:2180–96
45. Bovenschulte H, Krug B, Schneider T, et al. CT coronary angiography: coronary CT-flow quantification supplements morphological stenosis analysis. *Eur J Radiol*. 2013;82:608–16
46. Ko BS, Wong DT, Norgaard BL, et al. Diagnostic performance of transluminal attenuation gradient and noninvasive fractional flow reserve derived from 320-detector row CT angiography to diagnose hemodynamically significant coronary stenosis: an NXT substudy. *Radiology*. 2016;279:75–83
47. Lardo AC, Rahsepar AA, Seo JH, et al. Estimating coronary blood flow using CT transluminal attenuation flow encoding: formulation, preclinical validation, and clinical feasibility. *J Cardiovasc Comput Tomogr*. 2015;9:559–66. e1
48. Anderson HV, Stokes MJ, Leon M, Abu-Halawa SA, Stuart Y, Kirkeeide RL. Coronary artery flow velocity is related to lumen area and regional left ventricular mass. *Circulation*. 2000;102:48–54
49. Leone AM, De Caterina AR, Basile E, et al. Influence of the amount of myocardium subtended by a stenosis on fractional flow reserve. *Circ Cardiovasc Interv*. 2013;6:29–36
50. Dewey FE, Rosenthal D, Murphy DJ Jr, Froelicher VF, Ashley EA. Does size matter? Clinical applications of scaling cardiac size and function for body size. *Circulation*. 2008;117:2279–87
51. Seiler C, Kirkeeide RL, Gould KL. Measurement from arteriograms of regional myocardial bed size distal to any point in the coronary vascular tree for assessing anatomic area at risk. *J Am Coll Cardiol*. 1993;21:783–97

52. Huo Y, Kassab GS. Intraspecific scaling laws of vascular trees. *J R Soc Interface*. 2012;9:190–200
53. Kim HY, Lim HS, Doh JH, et al. Physiological severity of coronary artery stenosis depends on the amount of myocardial mass subtended by the coronary artery. *JACC Cardiovasc Interv*. 2016;9:1548–60
54. Kang SJ, Kweon J, Yang DH, et al. Mathematically derived criteria for detecting functionally significant stenoses using coronary computed tomographic angiography-based myocardial segmentation and intravascular ultrasound-measured minimal lumen area. *Am J Cardiol*. 2016;118:170–6
55. Sandoval Y, Smith SW, Thordsen SE, Apple FS. Supply/demand type 2 myocardial infarction: should we be paying more attention? *J Am Coll Cardiol*. 2014;63:2079–87
56. Gibbons RJ, Miller TD. Should extensive myocardial ischaemia prompt revascularization to improve outcomes in chronic coronary artery disease? *Eur Heart J*. 2015;36:2281–7
57. De Bruyne B, Fearon WF, Pijls NH, et al. Fractional flow reserve-guided PCI for stable coronary artery disease. *N Engl J Med*. 2014;371:1208–17
58. Johnson NP, Toth GG, Lai D, et al. Prognostic value of fractional flow reserve: linking physiologic severity to clinical outcomes. *J Am Coll Cardiol*. 2014;64:1641–54
59. Van Belle E, Rioufol G, Pouillot C, et al. Outcome impact of coronary revascularization strategy reclassification with fractional flow reserve at time of diagnostic angiography: insights from a large French multicenter fractional flow reserve registry. *Circulation*. 2014;129:173–85
60. Christakopoulos GE, Christopoulos G, Carlino M, et al. Meta-analysis of clinical outcomes of patients who underwent percutaneous coronary interventions for chronic total occlusions. *Am J Cardiol*. 2015;115:1367–75
61. Hachamovitch R, Hayes SW, Friedman JD, Cohen I, Berman DS. Comparison of the short-term survival benefit associated with revascularization compared with medical therapy in patients with no prior coronary artery disease undergoing stress myocardial perfusion single photon emission computed tomography. *Circulation*. 2003;107:2900–7
62. Chen SL, Ye F, Zhang JJ, et al. Randomized comparison of FFR-guided and angiography-guided provisional stenting of true coronary bifurcation lesions: the DKCRUSH-VI trial (double kissing crush versus provisional stenting technique for treatment of coronary bifurcation lesions VI). *JACC Cardiovasc Interv*. 2015;8:536–46
63. Ladwiniec A, Cunnington MS, Rossington J, et al. Collateral donor artery physiology and the influence of a chronic total occlusion on fractional flow reserve. *Circ Cardiovasc Interv*. 2015;8:e002219
64. Choi JH, Chang SA, Choi JO, et al. Frequency of myocardial infarction and its relationship to angiographic collateral flow in territories supplied by chronically occluded coronary arteries. *Circulation*. 2013;127:703–9
65. Ortiz-Perez JT, Rodriguez J, Meyers SN, Lee DC, Davidson C, Wu E. Correspondence between the 17-segment model and coronary arterial anatomy using contrast-enhanced cardiac magnetic resonance imaging. *JACC Cardiovasc Imaging*. 2008;1:282–93
66. Itu L, Rapaka S, Passerini T, et al. A machine-learning approach for computation of fractional flow reserve from coronary computed tomography. *J Appl Physiol*. 2016;121:42–52
67. Fokkema ML, James SK, Albertsson P, et al. Population trends in percutaneous coronary intervention: 20-year results from the SCAAR (Swedish coronary angiography and angioplasty registry). *J Am Coll Cardiol*. 2013;61:1222–30